Frontiers in Marine Science

TYPE Original Research
PUBLISHED 16 February 2023
DOI 10.3389/fmars.2023.1135911

Check for updates

OPEN ACCESS

EDITED BY
Toru Miyama,
Japan Agency for Marine-Earth Science and Technology, Japan

REVIEWED BY
Katsuto Uehara,
Kyushu University, Japan
Shinya Kouketsu,
Japan Agency for Marine-Earth Science and Technology (JAMSTEC), Japan

*CORRESPONDENCE
Zexun Wei
weizx@fio.org.cn

SPECIALTY SECTION
This article was submitted to Physical Oceanography, a section of the journal Frontiers in Marine Science

RECEIVED 02 January 2023
ACCEPTED 07 February 2023
PUBLISHED 16 February 2023

CITATION
Pan H, Sun J, Xu T, Teng F and Wei Z (2023) Seasonal variations of tidal currents in the deep Timor Passage. *Front. Mar. Sci.* 10:1135911. doi: 10.3389/fmars.2023.1135911

Seasonal variations of tidal currents in the deep Timor Passage

Haidong Pan[1,2,3,4], Junchuan Sun[1,2,3,4], Tengfei Xu[1,2,3,4], Fei Teng[1,2,3,4] and Zexun Wei[1,2,3,4]*

[1]Key Laboratory of Marine Science and Numerical Modeling, First Institute of Oceanography, Ministry of Natural Resources, Qingdao, China, [2]Laboratory for Regional Oceanography and Numerical Modeling, Qingdao, China, [3]Pilot National Laboratory for Marine Science and Technology, Qingdao, China, [4]Shandong Key Laboratory of Marine Science and Numerical Modeling, Qingdao, China

Exact knowledge on the seasonal variations of main tidal constituents is beneficial for improving tidal prediction. The semi-annual cycles in K_1 and S_2 tides are abnormally exaggerated by astronomical P_1 and K_2 tides, which interferes with our understanding on tidal seasonality. The widely-used tidal inference method in previous studies cannot fully separate astronomical P_1 and K_2 tides from seasonal P_1 and K_2 tides due to inaccurate inference relationship. In this study, on the basis of the 'credo of smoothness' which indicates that tidal admittances are smooth functions of tidal frequencies, we develop a novel but simple method to address this intractable issue and applied this method to explore the seasonality of tidal currents observed in the deep Timor Passage at the depth of 1800m. We find that the timing and range of seasonal modulations of M_2, S_2, K_1, and O_1 tides are distinct. Annual variations in tidal currents are much stronger than semi-annual variations in tidal currents. The annual and semi-annual ranges of M_2 tide can reach 2.69 cm/s and 1.51 cm/s, which are largest among main constituents. Although the annual range of K_1 tide is only 1.85 cm/s, considering the relatively small amplitude of time-averaged K_1 tide (2.87cm/s), K_1 the most affected tide by the annual cycle. The seasonal cycles of semi-diurnal tides (M_2 and S_2) are basically synchronous while those of diurnal tides (K_1 and O_1) are generally out-of-phase. As a general method, the proposed method can be widely applied to other sea areas to explore local tidal seasonality.

KEYWORDS

ocean tides, tidal currents, harmonic analysis, seasonal modulation, deep ocean

1 Introduction

Originated from astronomical forcing, tides and tidal currents are omnipresent in the global ocean and fundamental for ocean activities such as maritime logistics and ocean engineering (Amin, 1985; Pan et al., 2022a; Pan et al., 2022b; Wei et al., 2022). The interplay of barotropic tides with rough topography in the stratified ocean can generate baroclinic tides (Wunsch, 1975; Zhao et al., 2019). As an indispensable intermediate process in tide-to-turbulence cascade, baroclinic tides play a vital role in ocean mixing processes (Munk and Wunsch, 1998; Egbert and Ray, 2000; Li et al., 2021). Egbert and Ray (2000) indicated that deep sea mixing needs ~2TW energy to maintain deep-water circulation and at least 1TW energy is provided by baroclinic tides. As a result of seasonal changes in ocean environment (such as river flow, ocean stratification and sea ice), tides and tidal currents display significant seasonal variations which have been explored in the global ocean (Corkan, 1934; Foreman et al., 1995; Kang et al., 2002; St-Laurent et al., 2008; Kagan and Sofina, 2010; Georgas, 2012; Müller, 2012; Devlin et al., 2018; Wang et al., 2020; Du and Yu, 2021; Ray, 2022).

The seasonality of tidal currents in the deep sea are mainly derived from ocean stratification and astronomical factors (Xu et al., 2014; Cao et al., 2017; Li et al., 2021). The frequency of K_2 (P_1) tide is equal to that of the S_2 (K_1) tide add (minus) 2 cycle per year. Therefore, the semi-annual cycles of K_1 and S_2 tides are significantly enhanced due to the existence of astronomical P_1 and K_2 tides. To keep pace with the seasonal variations of M_2 and O_1 tides which are not influenced by nearby astronomical tides, nearly all researches applied tidal inference method to infer and eliminate the contribution of astronomical P_1 and K_2 tides when discussing the seasonal variations of K_1 and S_2 tides. The inference relationship between K_2 (P_1) and S_2 (K_1) tides can be determined based on the actual tidal constants from observed time series longer than half a year. It should be noted that the observed K_1 tide is nearly astronomical while the observed P_1 tide has two major energy sources: One is the astronomical P_1 tide, the another is the real seasonal variations of K_1 tide originated from semi-annual variations in ocean environment (labeled as the seasonal P_1 tide). Although the astronomical P_1 tide and the seasonal P_1 tide have same tidal period, their amplitudes and phases are totally different because they are forced by distinct physical processes (see section 3 for details). It is well known that astronomical P_1 and K_1 tidal waves have similar physical properties, thus, the astronomical P_1 tide can be simply inferred from the astronomical K_1 tide while the seasonal P_1 tide cannot. The observed P_1 tide is the vectorial synthesis of the seasonal P_1 tide and the astronomical P_1 tide. Similarly, the observed K_2 tide is the vectorial synthesis of the seasonal K_2 tide and the astronomical K_2 tide. Hence, the inference relationship derived from the observed P_1 (K_2) and observed K_1 (S_2) tide may be problematic due to the interference of the seasonal P_1 (K_2) tide.

To the best of our knowledge, there are no valid methods to take the place of the potentially problematic inference method to fully remove astronomical P_1 and K_2 tides from observed P_1 and K_2 tides. The aim of this research is to revisit this noteworthy issue and propose a new method according to the 'credo of smoothness' (Munk and Cartwright, 1966) to solve the problem. The new method is applied to the deep Timor Passage to explore the seasonality of local tidal currents. Our paper is organized as follows. Study area and tidal current observations are introduced in section 2. Section 3 displays the methods and results, followed by the discussions and conclusions in section 4 and section 5, respectively.

2 Study area and data

As a long, deep and narrow trench between the Australian continental shelf and the Timor Island with average depth of ~2000m (Figure 1), the Timor Passage is one of the major corridors for the Indonesian Throughflow (ITF). Fresh and warm sea waters from the western Pacific Ocean are transported to the tropical Indian Ocean *via* the Timor Passage and the Lombok and Ombai Straits, which are important and essential for maintaining the thermohaline balance in the global ocean (Sprintall et al., 2009). The deep current transport through the Timor Passage shows significant semi-annual and annual variations, which are related to remote Kelvin waves from the Indican Ocean and local monsoonal forcing, respectively (Wang et al., 2022).

Due to complex coastlines and topography, tides and tidal currents near the Indonesian archipelago are among the most complicated in the global ocean (Ray et al., 2005; Robertson, 2010). The mixing induced by tides has significant influences on ocean ecology and climate system (Sprintall and Révelard, 2014; Katavouta et al., 2022). Based on EOT20 tidal model (Hart-Davis et al., 2021) derived from multi-satellite altimeters, at the observation point, M_2 tide has the largest amplitude (88.39cm), followed by S_2 (48.78cm), K_1 (27.33cm), and O_1(17.00cm). Local tidal form factor, which is defined by the ratio of the sum of O_1 and K_1 tidal amplitudes to the sum of S_2 and M_2 tidal amplitudes (Pan et al., 2023a), is only 0.32, indicating that local tides are dominated by semi-diurnal tides.

Hourly current observations at depth of 1800m from the mooring (black dot in Figure 1) located in the southeast of the Timor Passage (122.9598°E, 11.3683°S) as part of the INSTANT program are analyzed. The Timor Passage mooring observations cover the period from January 1, 2004 to December 20, 2006. However, there are numerous missing values during January 1, 2004 to June 25, 2005. Thus, we only use 18 months observations from June 25, 2005 to December 20, 2006 to ensure the robustness and reliability of the results. The completeness of studied current data can reach 98.55%. More details of mooring observations can be found in Sprintall et al. (2009).

As shown in Figure 2, eastward tidal currents are significantly stronger than northward tidal currents due to the direction of the Timor Passage. Thus, we decompose eastward and northward currents into currents along and perpendicular to the trench. Only currents along the trench are focused and harmonically analyzed using S_TIDE toolbox (Pan et al., 2018a). It should be noted that to avoid the interference of strong non-tidal background currents on tidal estimation, we use Iteratively Reweighted Least Squares (IRLS) regression (Huber, 1996; Leffler and Jay, 2009) to take place of widely-used ordinary least squares (OLS) regression in the course of harmonic analysis. IRLS regression is much complicated than OLS regression and readers can refer Leffler and Jay (2009) for details. The effectiveness and accuracy of IRLS regression in tidal estimation have been verified by numerous studies (Leffler and Jay, 2009; Matte et al., 2013; Matte et al., 2014; Pan and Lv, 2021; Pan et al., 2022a; Pan et al., 2023a). Local tidal currents are highly non-stationary, with strong

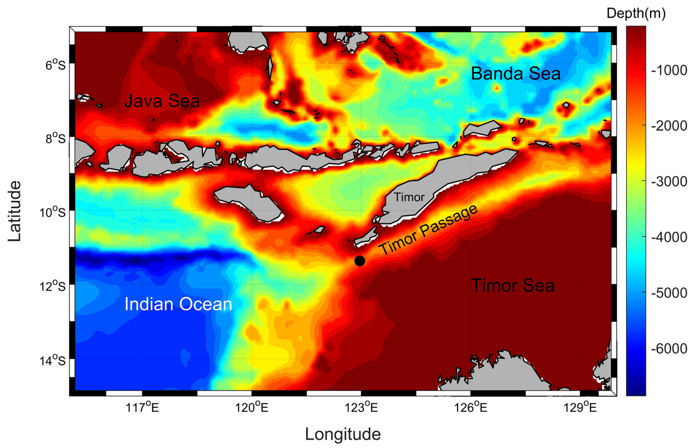

FIGURE 1
The location of the mooring (black dot). Water depths are from ETOPO1 dataset (Amante and Eakins, 2009).

intraseasonal vairiability (Figure 2), which deserves further investigation. Table 1 displays tidal constants of major tidal constituents in the deep Timor Passage. Ssa tide with a period of half a year has the largest amplitude (21.65cm/s). which is consistent with Wang et al. (2022). Sa tide with a period of a year has an amplitude of 4.27cm/s. Among semi-diurnal and diurnal tides, M_2 has the largest amplitude (9.05cm/s), followed by S_2 (4.38cm/s), K_1(2.87cm/s), and O_1(2.31cm/s).

Although long-period tides like Sa, Msm and Mf have large amplitudes, they are not significant due to low signal-to-noise ratios (SNRs). Generally, the SNR of a significant constituent should be no less than two (Pawlowicz et al., 2002). M_4 tide is the strongest shallow water constituent, with an amplitude of only 0.33cm/s. Figure 3A shows the combination of observed K_1, O_1, and P_1 tides. The sum of K_1 and O_1 tides can induce semi-monthly variations (13.66 days) of high tide. Note that P_1 tide can semi-annually modulate K_1 tide, thus, fortnightly variations of high tides (Figure 3A) are not stationary but modulated by semi-annual cycles. The combination of observed M_2, S_2, and K_2 tides also has semi-annually modulated fortnightly cycles (Figure 3B).

O_1 and Q_1 tidal frequencies are close, which means that O_1 and Q_1 tides have similar physical properties. As a result, tidal phase lags of O_1 and Q_1 tides are very close, and the difference of O_1 and Q_1 tidal phase lags is only 3.76° (Table 1). The difference of K_1 and P_1 frequencies is much smaller than that of O_1 and Q_1 frequencies, which means that the difference of K_1 and P_1 phase lags should be

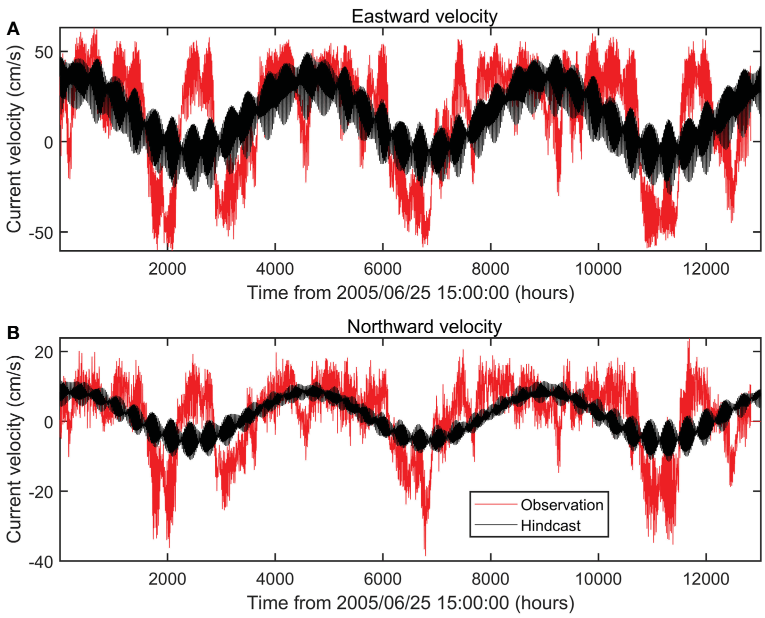

FIGURE 2
(A) Eastward current velocities (red line) and their hindcast (black line) *via* harmonic analysis. **(B)** Northward current velocities (red line) and their hindcast (black line) *via* harmonic analysis.

TABLE 1 Amplitudes and phase lags of major diurnal, semi-diurnal, and shallow water tides estimated from long-term current observations along the trench. SNR means signal-to-noise ratio.

Constituent	Frequency ($hour^{-1}$)	Amplitude(cm/s)	Phase (degree)	SNR
Sa	0.0001141	4.2680	163.46	0.5
Ssa	0.0002282	21.6476	207.68	8.1
Msm	0.0013098	3.5033	295.39	0.3
Mm	0.0015122	1.4871	44.85	0.1
Msf	0.0028219	1.6617	42.94	0.1
Mf	0.0030501	2.1177	102.77	0.2
Q_1	0.0372185	0.5917	110.85	7.7
O_1	0.0387307	2.3090	114.61	100
P_1	0.0415526	1.0154	130.69	14
K_1	0.0417807	2.8669	142.01	170
N_2	0.0789992	1.7850	38.29	18
M_2	0.0805114	9.0524	70.40	410
S_2	0.0833333	4.3787	124.75	100
K_2	0.0835615	1.2775	128.86	13
MK_3	0.1222921	0.1334	87.91	1.2
M_4	0.1610228	0.3306	50.83	3.1
MS_4	0.1638447	0.1867	158.68	1.1
M_8	0.3220456	0.0278	249.47	1.5

smaller than 3.76°. However, the observed difference of K_1 and P_1 phase lags is as high as 11.32°, which clearly indicates that the observed P_1 tide is not purely astronomical, but contains a non-negligible contribution of K_1 seasonality. In the next section, we will introduce a novel method which can fully separate the seasonal P_1 (K_2) tide from the astronomical P_1 (K_2) tide.

3 Methodology and results

3.1 Methodology

The proposed method is based on the 'credo of smoothness' (Munk and Cartwright, 1966) which implies that tidal admittances

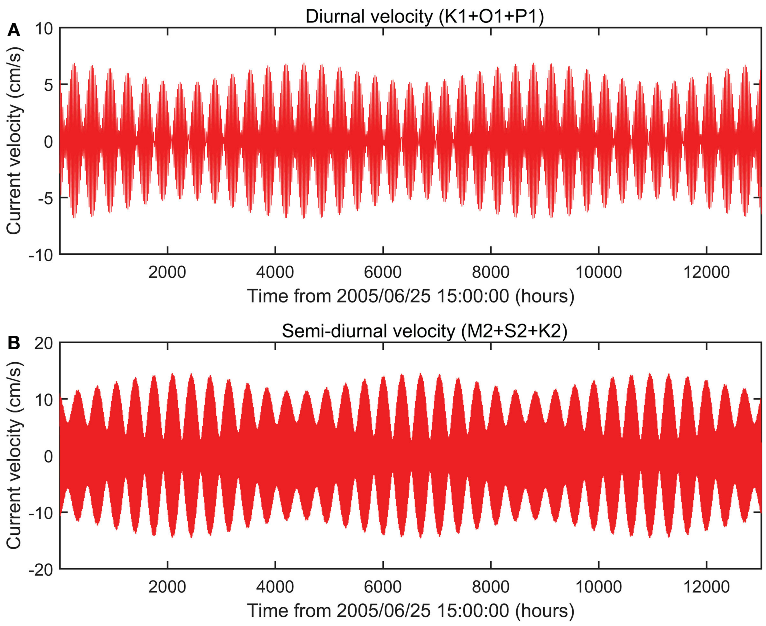

FIGURE 3
(A) The combination of observed K_1, O_1, and P_1 tidal currents. **(B)** The combination of observed M_2, S_2, and K_2 tidal currents. Note that the results are estimated from currents along the trench.

are smooth functions of tidal frequencies (Feng et al., 2015; Pan et al., 2023b). Defined by the ratios of observed amplitudes to equilibrium amplitudes (normalized amplitude) and phase differences of observed phases and equilibrium phases, tidal admittances represent the response of astronomical forcing to local topography and coastlines. In general, tidal waves with close periods always have similar responses which means that their admittances should also be close. Note that such smoothness is built on the premise that tides are purely astronomical. The existence of non-astronomical tides may destroy the nature of smoothness, but also provides an opportunity to eliminate non-astronomical tides.

Equilibrium tidal amplitudes are obtained *via* s_equilibrium_tide function in S_TIDE toolbox. Phase differences of observed phases and equilibrium phases (i.e. phase lags) are directly estimated *via* classical harmonic analysis. The admittances of minor tidal constituents such as J_1, $2Q_1$, $2N_2$, L_2 are not used because their SNRs are too small (generally less than 0.5) which means that they may be contaminated by strong non-tidal background noises. As shown in Figure 4A, normalized diurnal amplitudes are parabolic functions of tidal frequencies (dash line). Unknown coefficients (i.e. a, b, c) in Eq.(1) can be estimated by ordinary least squares. f is tidal frequency. Cubic polynomials or higher-order polynomials are not recommended to avoid over-fitting(Feng et al., 2015; Pan et al., 2023b).

$$y = a + bf + cf^2 \tag{1}$$

Due to the interfere of non-astronomical contributions, normalized observed P_1 amplitude significantly deviates from the fitting curve. Similarly, phase differences are also quadratic functions of frequencies (Figure 4B). The observed P_1 phase difference noticeably deviates from the quadratic curve. By the quadratic interpolation, the normalized astronomical P_1 amplitude and astronomical P_1 phase difference can be calculated (red dots in Figure 4). Based on known equilibrium amplitudes, the astronomical P_1 amplitude (0.90 cm/s) and phase lag (139.04°) are calculated. The astronomical P_1 phase lag (139.04°) is very close to the astronomical K_1 phase lag (142.01°). The ratio of the astronomical P_1 amplitude (0.90 cm/s) to the astronomical K_1 amplitude (2.87cm/s) is 0.314 which is slightly smaller than the equilibrium theoretical value (0.331). At last, subtracting the astronomical P_1 tide vectorially from the observed P_1 tide generates the seasonal P_1 tide (Figure 5A). The amplitude and phase of the seasonal P_1 tide is 0.181cm/s and 84.4°, respectively.

As displayed in Figure 6A, normalized semi-diurnal amplitudes range from 0.55 to 0.6 except K_2. Phase differences for semi-diurnal tides are nearly linear (Figure 6B). Based on the fitting curve and equilibrium amplitudes, the astronomical K_2 amplitude (1.221cm/s) and phase lag (129.72°) are calculated. *Via* vector operation, the seasonal K_2 amplitude (0.06cm/s) and phase lag (110.93°) are derived. Because the seasonal K_2 tide is very weak, therefore, the observed K_2 tide is nearly same to the astronomical K_2 tide (Figure 5B).

3.2 Seasonal variations of main tidal constituents

The seasonality of main tidal constituents can induce minor constituents whose frequencies are near main constituents. For example, the annual modulation of K_1 tide can induce S_1 and PSI_1 tides, whose frequencies are w_{K1}-w_{Sa} and w_{K1}+w_{Sa}, where w_{K1} and w_{Sa} mean the frequencies of K_1 and Sa tides, respectively. The semi-annual modulation of K_1 tide can induce P_1 and PHI_1 tides, whose

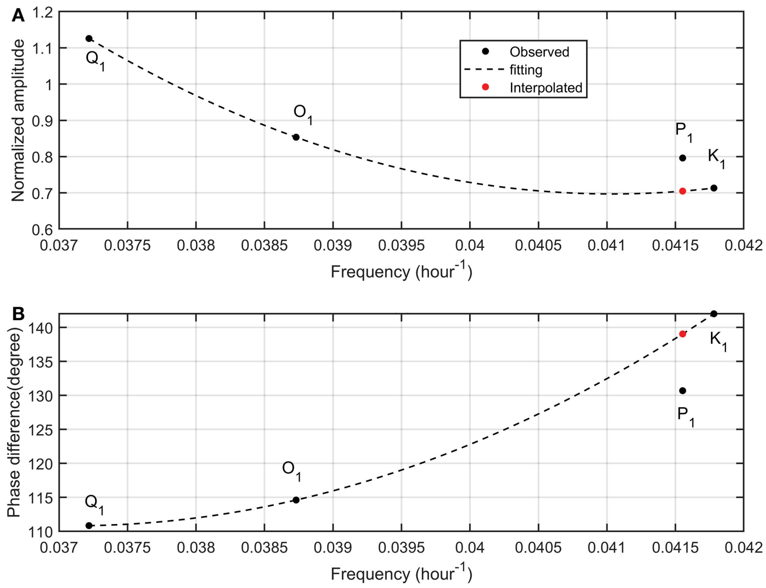

FIGURE 4
Normalized tidal amplitudes **(A)** and phase differences **(B)** for main diurnal tides at depth of 1800m from the mooring. Black dots are observed tidal admittances while red dots are interpolated admittances. Dash lines are determined *via* ordinary least squares.

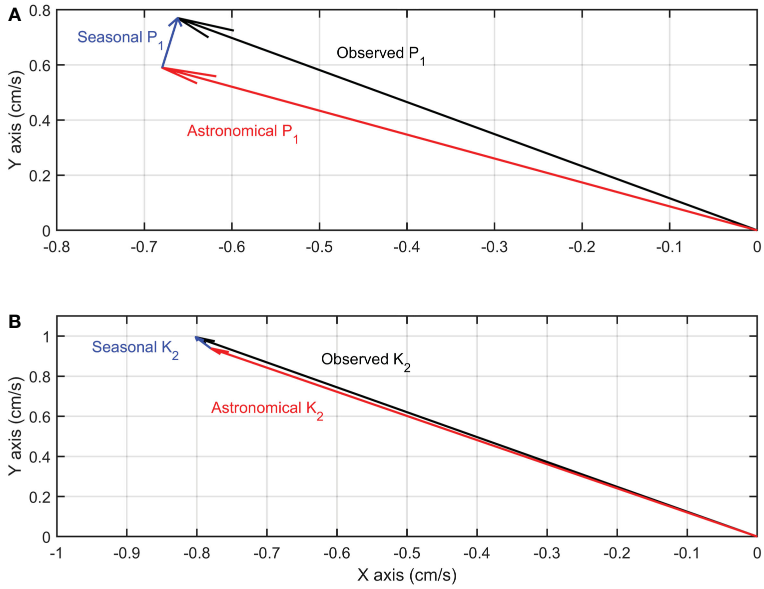

FIGURE 5
(A) The vectorial synthesis of the seasonal P_1 tide (blue arrow) and the astronomical P_1 tide (red arrow) generates the observed P_1 tide (black arrow). **(B)** Same as A, but for K_2 tide.

frequencies are w_{K1}-2*w_{Sa} and w_{K1}+2*w_{Sa}. The annual modulation of S_2 tide can induce T_2 and R_2 tides, whose frequencies are w_{S2}-w_{Sa} and w_{S2}+w_{Sa}. Like P_1 and K_2, T_2 tide can also directly obtain considerable energy from astronomical forcing. According to the fitting curve in Figure 6, the astronomical T_2 amplitude (0.256cm/s) and phase lag (122.93°) can be calculated. The observed T_2 amplitude and phase lag are 0.578cm/s and 182.03°, respectively. Through vectorial operation, the seasonal T_2 amplitude (0.498cm/s) and phase lag (208.22°) are obtained.

The combination of S_1 and PSI_1 tides represents the annual cycle of K_1 tide while the combination of P_1 (astronomical contribution removed) and PHI_1 tides represents the semi-annual cycle of K_1 tide (Figure 7). The seasonal variations of M_2, S_2, and O_1 tides can be obtained in similar ways (Figures 7, 8). As shown in Figures 7, 8, seasonal variations of four main constituents are significant and their features are distinct. M_2 tide has the largest annual range (2.69cm/s), followed by S_2 (1.85cm/s), K_1 (1.85cm/s), and O_1 (0.93cm/s). Considering the

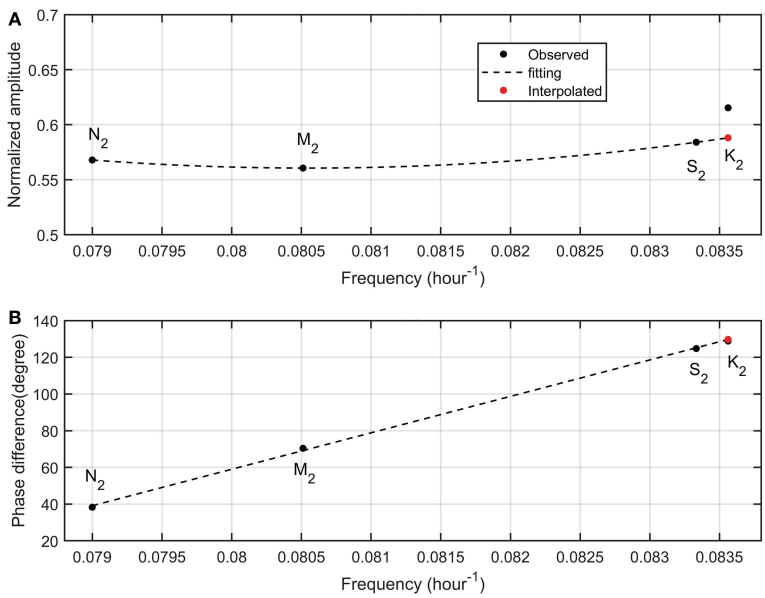

FIGURE 6
Same as Figure 4, but for semi-diurnal tides.

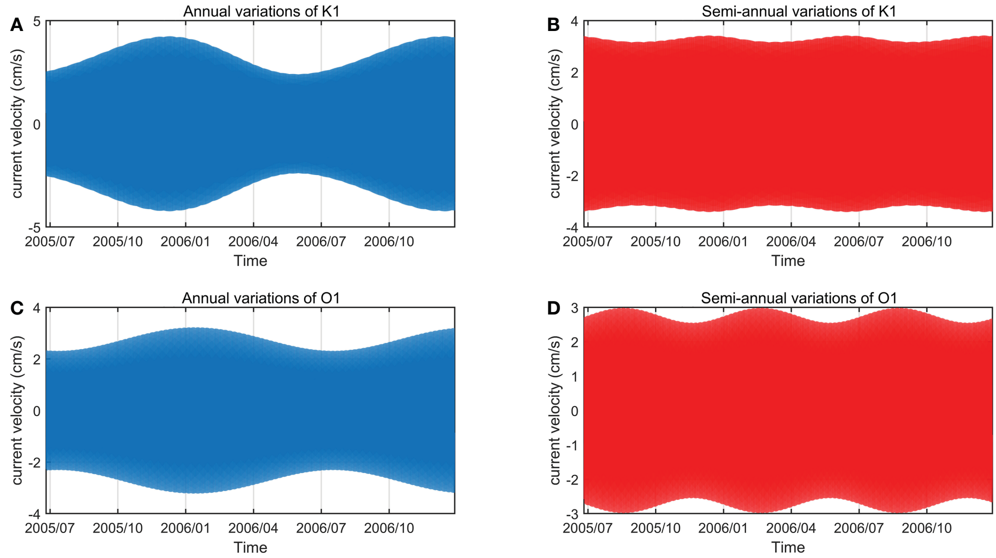

FIGURE 7
Annual **(A)** and semi-annual **(B)** variations of K_1 tidal currents. Annual **(C)** and semi-annual **(D)** variations of O_1 tidal currents.

relatively small amplitude of K_1 tide (2.87cm/s), it is the greatest affected tide by the annual cycle. The range of the semi-annual cycle is much smaller than that of the annual cycle. M_2 tide has the largest semi-annual range (1.51cm/s), followed by S_2 (0.72cm/s), O_1 (0.45cm/s), and K_1 (0.27cm/s). Among four major tidal constituents, O_1 tide has the largest ratio of the range of the semi-annual cycle to tidal amplitude (0.195), which means that the semi-annual cycle has the strongest influence on O_1 tide.

The annual variations of M_2 and S_2 tides are precisely synchronous (Figure 8). Both of them peak at the end of September while reach the minimum value in early April. Compared to semi-diurnal tides, the annual variations of K_1 and O_1 tides are basically synchronous (Figure 7). K_1 tide peaks in early December while reach the minimum value at the end of May. The annual variation of O_1 tide has a delay of about one month compared to that of K_1 tide.

The semi-annual variations of K_1 and O_1 tides are generally opposite. The semi-annual variation of K_1 reaches the minimum value at the end of August and peaks in early December while that of O_1 peaks in mid-August and reaches the minimum value in mid-December (Figure 7). The semi-annual variations of M_2 and S_2 tides are generally synchronous while a delay of about 20 days exists (Figure 8). The semi-annual variation of M_2 reaches the minimum value at the end of December and peaks at the end of September while that of S_2 peaks in early September and reaches

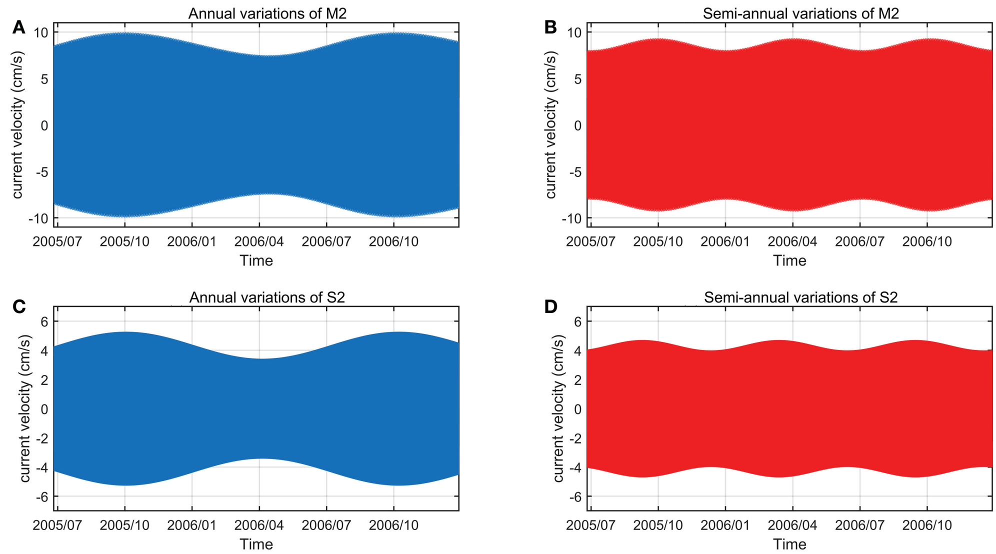

FIGURE 8
Annual **(A)** and semi-annual **(B)** variations of M_2 tidal currents. Annual **(C)** and semi-annual **(D)** variations of S_2 tidal currents.

the minimum value in early December. Figures 7, 8 indicate that tidal response to seasonal changes in ocean environment is frequency-dependent.

4 Discussions

4.1 Application to surface tides

The proposed method is not limited to deep currents but can also be applied to surface tides because the principle of smoothness is generally credible for all tidal signals. Surface tides at the mooring also have noticeable seasonal variations. Figures 9, 10 display tidal admittances for main semi-diurnal and diurnal tides which are totally different. Tidal admittances for diurnal tides are parabolic functions of tidal frequencies while those for semi-diurnal tides are nearly linear functions. The structure of functions should be related to the local topography and coastline which can influence tidal propagation, reflection, refraction, and dissipation. It is obvious that diurnal tides and semi-diurnal tides which have vastly different periods and wave lengths must show distinct tidal responses to the astronomical forcing in the same sea areas.

Like tidal currents, the seasonality of surface tides makes P_1 and K_2 tidal admittances deviate from the fitted curves. Based on the method described above, the seasonal P_1 (K_2) tide can be separated from the astronomical P_1 (K_2) tide. The seasonal (astronomical) P_1 tide has an amplitude of 0.46 (8.44) cm and a phase lag of 34.32° (175.64°) while the seasonal (astronomical) K_2 tide has an amplitude of 1.49 (13.69) cm and a phase lag of 37.02° (126.56°). The ratio of the astronomical P_1 amplitude (8.44cm) to the astronomical K_1 amplitude (27.33cm) is 0.309 which indicates that tidal inference using the equilibrium theoretical value (0.331) may be not accurate enough even in the deep sea.

4.2 Limitation of the proposed method

Near-inertial currents are generated by ubiquitous changing wind stress (Munk and Wunsch, 1998; Hu et al., 2023). The frequency of near-inertial currents is near F (i.e. Coriolis frequency), which can be expressed as following:

$$F = 2w \sin(L) \quad (2)$$

Where L is latitude while w is the angular velocity of the earth rotation. It is obvious that the period of near-inertial currents changes with latitude. At 26.45°N/S, 27.61°N/S, 29.82°N/S, 30.00° N/S, the periods of near-inertial currents are same to the periods of Q_1, O_1, P_1, and K_1 tides, respectively. Also, at 70.98°N/S, 74.48°N/S. 85.78°N/S, the periods of near-inertial currents are same to the periods of N_2, M_2 and S_2 tides. Therefore, at these latitudes, near-inertial motions can contribute to semi-diurnal and diurnal tides, and the credo of smoothness may be interfered. Note that no near-inertial motions can contribute to K_2 tide.

In addition, in the development of the principle of smoothness, Munk and Cartwright (1966) did not consider the potential influence of tidal resonance which may influence the smoothness of tidal admittances. Hence, care must be taken when applying the proposed method to resonant sea areas, such as the Gulf of Tonkin in the South China Sea, which is well-known for strong diurnal resonance (Pan et al., 2022a; Pan et al., 2023a).

5 Conclusions and summary

Tides and tidal currents display noticeable seasonal variability in numerous sea areas especially in the river estuaries and polar regions. Knowledge on tidal seasonality is fundamental for accurate tidal prediction which is beneficial for substantial human activities

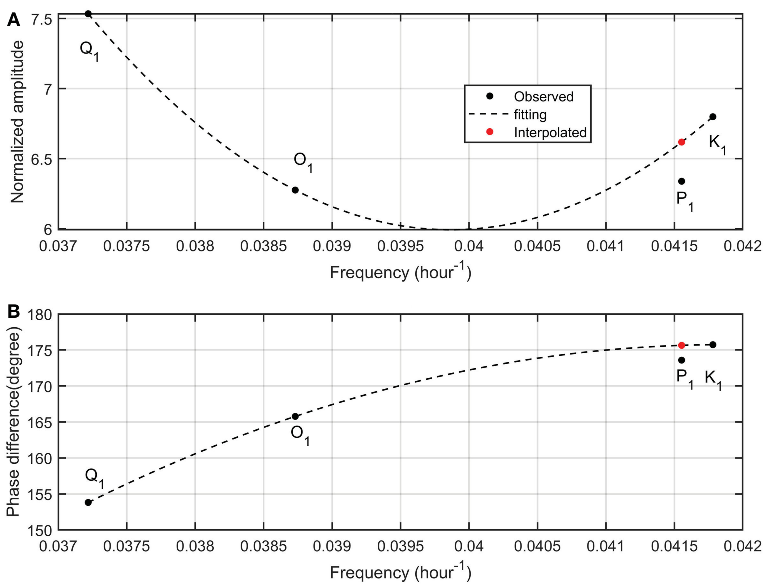

FIGURE 9
Same as Figure 4, but for surface tides at the mooring. Tidal constants are derived from EOT20 model.

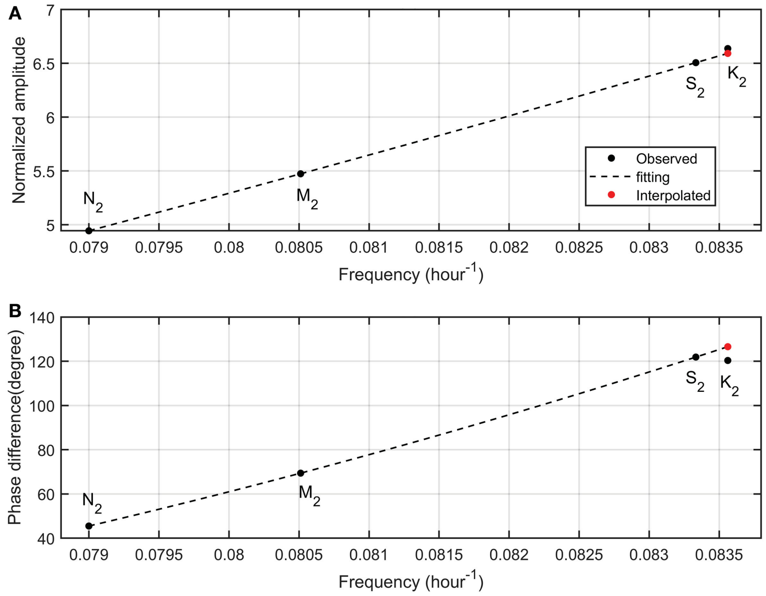

FIGURE 10
Same as Figure 6, but for surface tides at the mooring. Tidal constants are derived from EOT20 model.

in the ocean like navigation and ocean engineering (Müller et al., 2014; Pan et al., 2018a; Pan et al., 2018b; Gan et al., 2021; Pan and Lv, 2021; Wei et al., 2022). Due to different tidal periods and wave lengths, the seasonal variations of main tidal constituents are distinct. The existence of astronomical P_1 and K_2 tides anomalously exaggerate the semi-annual cycles in K_1 and S_2 tides. The method of tidal inference which is widely used in previous studies cannot fully separate astronomical P_1 and K_2 tides from seasonal P_1 and K_2 tides. In this research, a novel but simple method based on the 'credo of smoothness' is developed to solve this nettlesome problem. Since tidal admittances are smooth functions of frequencies, astronomical P_1 and K_2 tides can be obtained *via* the interpolation. The seasonal P_1 (K_2) tide has totally different amplitude and phase compared to the astronomical P_1 (K_2) tide.

We applied the proposed method to explore the seasonality of tidal currents observed in the deep Timor Passage at the depth of 1800m. It is found that the timing and range of seasonal variations of four main constituents are discrepant. The annual and semi-annual ranges of M_2 tide are largest among main constituents. O_1 tide has the smallest annual range while K_1 has the smallest semi-annual range. The peak times of seasonal variations of M_2 and S_2 tides are generally consistent while those of K_1 and O_1 tides are basically not synchronous. Except tidal currents in the deep sea, our method is also suitable for surface tides. It is expected that the proposed method can be widely used in the exploration of tidal seasonality in the global ocean.

Data availability statement

The original contributions presented in the study are included in the article/supplementary material. Further inquiries can be directed to the corresponding author.

Author contributions

HP: Data curation, Conceptualization, Methodology, Visualization, Writing – original draft, Writing – review & editing. JS, TX, FT: Writing – review & editing. ZW: Writing – review & editing, Supervision, Resources, Funding acquisition. All authors contributed to the article and approved the submitted version.

Funding

This study is jointly supported by the Laoshan Laboratory (No. LSKJ202202700), the National Natural Science Foundation of China (NSFC) Projects (42206022, 42076024, 42076023), the Global Change and Air-Sea Interaction II (Contact No.GASI-01-ATP-STwin), the China Postdoctoral Science Foundation (2022M713677) and the Qingdao postdoctoral application research project (QDBSH202108).

Conflict of interest

The authors declare that the research was conducted in the absence of any commercial or financial relationships that could be construed as a potential conflict of interest.

Publisher's note

References

Amante, C., and Eakins, B. W. (2009). ETOPO1 1 arc-minute global relief model: Procedures, data sources and analysis. *NOAA Tech. Memorandum NESDIS NGDC-24*, 19.

Amin, M. (1985). Temporal variations of tides on the west coast of great Britain. *Geophys. J. R. Astron. Soc.* 82, 279–299. doi: 10.1111/j.1365-246X.1985.tb05138.x

Cao, A., Guo, Z., Lv, X., Song, J., and Zhang, J. (2017). Coherent and incoherent features, seasonal behaviors and spatial variations of internal tides in the northern south China Sea. *J. Mar. Syst.* 172, 75–83. doi: 10.1016/j.jmarsys.2017.03.005

Corkan, R. H. (1934). An annual perturbation in the range of tide. *P. R. Soc London* 144, 537–559. doi: 10.2307/2935543

Devlin, A. T., Zaron, E. D., Jay, D. A., and Talke, S. (2018). Seasonality of tides in southeast Asian waters. *J. Phys. Oceanogr.* 48 (2), 1169–1190. doi: 10.1175/JPO-D-17-0119.1

Du, Z., and Yu, Q. (2021). Comment on "seasonal and nodal variations of predominant tidal constituents in the global ocean". *Cont. Shelf Res.* 227, 104524. doi: 10.1016/j.csr.2021.104524

Egbert, G. D., and Ray, R. D. (2000). Significant dissipation of tidal energy in the deep ocean inferred from satellite altimeter data. *Nature* 405, 775–778. doi: 10.1038/35015531

Feng, X., Tsimplis, M. N., and Woodworth, P. L. (2015). Nodal variations and long-term changes in the main tides on the coasts of China. *J. Geophys. Res. Oceans* 120, 1215–1232. doi: 10.1002/2014JC010312

Foreman, M. G. G., Walters, R. A., Henry, R. F., Keller, C. P., and Dolling, A. G. (1995). A tidal model for eastern Juan de fuca strait and the southern strait of Georgia. *J. Geophys. Res. Oceans* 100, 721–740. doi: 10.1029/94JC02721

Gan, M., Pan, H., Chen, Y., and Pan, S. (2021). Application of the variational mode decomposition (VMD) method to river tides. *Estuar. Coast. Shelf Sci.* 261, 107570. doi: 10.1016/j.ecss.2021.107570

Georgas, N. (2012). Large Seasonal modulation of tides due to ice cover friction in a midlatitude estuary. *J. Phys. Oceanogr.* 42, 352–369. doi: 10.1175/JPO-D-11-063.1

Hart-Davis, M. G., Piccioni, G., Dettmering, D., Schwatke, C., Passaro, M., and Seitz, F. (2021). EOT20: a global ocean tide model from multi-mission satellite altimetry, earth syst. *Sci. Data* 13, 3869–3884. doi: 10.5194/essd-13-3869-2021

Hu, Y., Yu, F., Chen, Z., Si, G., Liu, X., and F and Ren, Q. (2023). Two near-inertial peaks in antiphase controlled by stratification and tides in the yellow Sea. *Front. Mar. Sci.* 9, 1081869. doi: 10.3389/fmars.2022.1081869

Huber, P. J. (1996). Robust statistical procedures, CBMS-NSF regional conference series in applied mathematics, vol. 68, 2nd ed. *Soc. Ind. Appl. Mathematics*, 67.

Kagan, B., and Sofina, E. (2010). Ice-induced seasonal variability of tidal constants in the Arctic ocean. *Cont. Shelf Res.* 30, 643–647. doi: 10.1016/j.csr.2009.05.010

Kang, S. K., Foreman, M. G. G., Lie, H.-J., Lee, J.-H., Cherniawsky, J., and Yum, K.-D. (2002). Two-layer tidal modeling of the yellow and East China seas with application to seasonal variability of the M_2 tide. *J. Geophys. Res.* 107 (C3), 3020. doi: 10.1029/2001JC000838

Katavouta, A., Polton, J. A., Harle, J. D., and Holt, J. T. (2022). Effect of tides on the Indonesian seas circulation and their role on the volume, heat and salt transports of the Indonesian throughflow. *J. Geophys. Res. Oceans* 127, e2022JC018524. doi: 10.1029/2022JC018524

Leffler, K. E., and Jay, D. A. (2009). Enhancing tidal harmonic analysis: Robust (hybrid L1/L2) solutions. *Cont. Shelf Res.* 29 (1), 78–88. doi: 10.1016/j.csr.2008.04.011

Li, B., Wei, Z., Wang, Y., Guo, X., Xu, T., and Lv, X. (2021). Application of S_TIDE in exploration of seasonal variations of internal tidal amplitudes in the northern south China Sea. *J. Atmos. Oceanic Technol.* 38, 1425–1438. doi: 10.1175/JTECH-D-20-0119.1

Matte, P., Jay, D. A., and Zaron, E. D. (2013). Adaptation of classical tidal harmonic analysis to nonstationary tides, with application to river tides. *J. Atmos. Ocean. Technol.* 30, 569–589. doi: 10.1175/JTECH-D-12-00016.1

Matte, P., Secretan, Y., and Morin, J. (2014). Temporal and spatial variability of tidal-fluvial dynamics in the st. Lawrence fluvial estuary: An application of nonstationary tidal harmonic analysis. *J. Geophys. Res. Oceans* 119, 5724–5744. doi: 10.1002/2014JC009791

Müller, M. (2012). The influence of changing stratification conditions on barotropic tidal transport and its implications for seasonal and secular changes of tides, cont. *Shelf Res.* 47, 107–118. doi: 10.1016/j.csr.2012.07.003

Müller, M., Cherniawsky, J. Y., Foreman, M. G., and von Storch, J.-S. (2014). Seasonal variation of the M_2 tide. *Ocean Dynam.* 64, 159–177. doi: 10.1007/s10236-013-0679-0

Munk, W. H., and Cartwright, D. E. (1966). Tidal spectroscopy and prediction. *Philos. Trans. R. Soc London A* 259, 533–581. doi: 10.1098/rsta.1966.0024

Munk, W., and Wunsch, C. (1998). Abyssal recipes II: Energetics of tidal and wind mixing. *Deep-Sea Res. Part I-Oceanogr Res. Pap* 45, 1977–2010. doi: 10.1016/S0967-0637(98)00070-3

Pan, H., Devlin, A. T., Xu, T., Lv, X., and Wei, Z. (2022a). Anomalous 18.61-year nodal cycles in the gulf of tonkin revealed by tide gauges and satellite altimeter records. *Remote Sens.* 14, 3672. doi: 10.3390/rs14153672

Pan, H., Guo, Z., Wang, Y., and Lv, X. (2018b). Application of the EMD method to river tides. *J. Atmos. Oceanic Technol.* 35 (4), 809–819. doi: 10.1175/JTECH-D-17-0185.1

Pan, H., Jiao, S., Xu, T., Lv, X., and Wei, Z. (2022b). Investigation of tidal evolution in the bohai Sea using the combination of satellite altimeter records and numerical models. *Estuar. Coast. Shelf Sci.* 279, 108140. doi: 10.1016/j.ecss.2022.108140

Pan, H., Li, B., Xu, T., and Wei, Z. (2023a). Subseasonal tidal variability in the gulf of tonkin observed by multi-satellite altimeters and tide gauges. *Remote Sens.* 15, 466. doi: 10.3390/rs15020466

Pan, H., and Lv, X. (2021). Is there a quasi 60-year oscillation in global tides? *Cont. Shelf Res.* 222, 104433. doi: 10.1016/j.csr.2021.104433

Pan, H., Lv, X., Wang, Y., Matte, P., Chen, H., and Jin, G. (2018a). Exploration of tidal-fluvial interaction in the Columbia river estuary using S_TIDE. *J. Geophys. Res. Oceans* 123, 6598–6619. doi: 10.1029/2018JC014146

Pan, H., Xu, T., and Wei, Z. (2023b). Anomalously large seasonal modulations of shallow water tides at lamu, Kenya. *Estuar. Coast. Shelf Sci.* 281, 108203. doi: 10.1016/j.ecss.2022.108203

Pawlowicz, R., Beardsley, B., and Lentz, S. (2002). Classical tidal harmonic analysis including error estimates in MATLAB using T_TIDE. *Comput. Geosci.* 28 (8), 929–937. doi: 10.1016/S0098-3004(02)00013-4

Ray, R. D. (2022). Technical note: On seasonal variability of the M_2 tide. *Ocean Sci.* 18, 1073–1079. doi: 10.5194/os-18-1073-2022

Ray, R. D., Egbert, G. D., and Erofeeva, S. Y. (2005). A brief overview of tides in the Indonesian seas. *Oceanography* 18, 74–79. doi: 10.5670/oceanog.2005.07

Robertson, R. (2010). Tidal currents and mixing at the INSTANT mooring locations. *Dynam. Atmos. Oceans* 50, 331–373. doi: 10.1016/j.dynatmoce.2010.02.004

Sprintall, J., and Révelard, A. (2014). The Indonesian throughflow response to indo-pacific climate variability. *J. Geophys. Res. Oceans* 119 (2), 1161–1175. doi: 10.1002/2013JC009533

Sprintall, J., Wijffels, S. E., Molcard, R., and Jaya, I. (2009). Direct estimates of the Indonesian throughflow entering the Indian ocean: 2004-2006. *J. Geophys. Res.* 114, C07001. doi: 10.1029/2008JC005257

St-Laurent, P., Saucier, F. J., and Dumais, J.-F. (2008). On the modification of tides in a seasonally ice-covered sea. *J. Geophys. Res.* 113, C11014. doi: 10.1029/2007JC004614

Wang, D., Pan, H., Jin, G., and Lv, X. (2020). Seasonal variation of the main tidal constituents in the bohai bay. *Ocean Sci.* 16, 1–14. doi: 10.5194/os-16-1-2020

Wang, J., Zhang, Z., Li, X., Wang, Z., Li, Y., Hao, J., et al. (2022). Moored observations of the timor passage currents in the Indonesian seas. *J. Geophys. Res. Oceans* 127, e2022JC018694. doi: 10.1029/2022JC018694

Wei, Z., Pan, H., Xu, T., Wang, Y., and Wang, J. (2022). Development history of the numerical simulation of tides in the East Asian marginal seas: An overview. *J. Mar. Sci. Eng.* 10, 984. doi: 10.3390/jmse10070984

Wunsch, C. (1975). Internal tides in the ocean. *Rev. Geophys.* 13, 167–182. doi: 10.1029/RG013i001p00167

Xu, Z., Yin, B., Hou, Y., and Liu, A. K. (2014). Seasonal variability and north-south asymmetry of internal tides in the deep basin west of the Luzon strait. *J. Mar. Syst.* 134, 101–112. doi: 10.1016/j.jmarsys.2014.03.002

Zhao, J., Zhang, Y., Liu, Z., Zhao, Y., and Wang, M. (2019). Seasonal variability of tides in the deep northern south China Sea. *Sci. China Earth Sci.* 62, 671–783. doi: 10.1007/s11430-017-9315-7